Academy journal for Basic and Applied Sciences (AJBAS) Volume 7 issue 1, 2025..

The impact of Scattering Correction Techniques on The performance of Gamma Camera

D. Dabos[1], M.A.Koshlaf[2], N.M.Alteef[3] , A.Kushada[4]

1. Physics Department, School of Basic Science , Libyan Academy.
2. Libyan Medical Research Center, Alzaweya .
3. Physics Department, Alzytona University.
4. Radiology Department, Faculty of Medicine, Azweya University.

Mona.Koshlaf@academy.edu.Ly

Abstract: In nuclear medicine, scattering correction plays a crucial role in improving the accuracy and reliability of diagnostic imaging techniques such as nuclear medicines such as single -photon emission computed tomography (SPECT) .

The main aim of measuring scattering correction in gamma camera is to improve the accuracy and reliability of diagnostic images.

Correction was made for attenuation by transmission measurements. Three different scatter correction methods were used; the Triple Energy Window method (TEW), the Double Energy Window method (DEW) and the Lower Energy Window method (LEW).

The scatter correction gave an underestimation ranging between 20% and 0.5 % (for ^{99m}Tc and all organs) depending on the correction methods used. For ^{123}I, these values ranged between an overestimation of 14% and 1.2 %. For higher background activities, the deviation from the true activity values became higher, but reasonably accurate. The most consequent results when considering all organs and organ-to-background activities was found when applying the LEW scatter correction method combined with the Bujis background correction method.

^{123}I is the most accurate results of attenuation and scatter correction was obtained for large organs when applying the TEW method.

Keywords: scatter correction, gamma camera, attenuation, energy window.

I. INTRODUCTION

Scattered photons pose a significant challenge in conventional scintigraphic imaging and single photon emission computed tomography (SPECT), leading to inaccuracies in event positioning and reduced image quality. These unwanted events introduce low-frequency blurring, diminishing image contrast and impacting lesion detection in qualitative imaging. Moreover, in quantitative imaging, scattered events can cause substantial errors in evaluating regional radionuclide concentrations.

Historically, one method to mitigate the impact of scattered events was to increase the lower threshold of the energy discrimination window towards the total absorption peak's upper range. While this approach is suitable for SPECT, it has drawbacks—scattered photon interference remains high, while primary event numbers may decrease significantly, resulting in blurred images that hinder both qualitative and quantitative assessments.

Recent advancements in scatter correction techniques involve subtracting events in a manner that aligns with the actual distribution of scattered events within acquired images. The quantity and dispersion of scattered photons can be determined using Monte-Carlo simulation computer code or alternative mathematical models. [1-2]

DOI:10.5281/zenodo.15085839

Numerous scatter correction methods have been proposed, indicating an ongoing area of research. Despite various approaches, there is no universally accepted technique, although the triple energy window or dual energy window methods are prevalently utilized. Other groups have explored alternative strategies such as multiple energy windows, convolution subtraction, or intricate scatter modeling. [3-4].

III. MATERIAL AND METHODS

In this work we present results on the following properties of the Skylight Philips Dual Head gamma camera: energy resolution, sensitivity, spatial resolution and **i**maging evaluation. Except for energy resolution other situations correspond events selected within an energy window centered on the ^{99m}Tc photopeak (130 – 149 keV). The images were reconstructed in matrices of 1024 × 1024 pixels, with a pixel size of 0.6 mm.

In the present work we also use Monte Carlo simulation (Geant4 simulation) [12] to check on some of gamma camera characteristics announced by the manufacturer.

1- Energy resolution

The energy resolution of the gamma camera was measured with a ^{99m}Tc point source (activity of 1.8×10^6 Bq) placed at the center of the field of view (FOV), 10 cm apart the crystal surface. The energy spectrum was acquired for 2 minutes.

This setup was simulated for photons generated with a normal incidence to the crystal in order to simulate an ideal collimator. The simulated and the experimental energy spectra obtained are shown in figure-1 and figure-2, respectively. Some differences may be observed between them, the most striking being that the experimental spectrum presents a wider peak which may be explained by the superposition of the energy peaks corresponding to the γ-ray escape of 53I present in the NaI(Tl) crystal (~110 keV), the ^{99m}Tc photopeak (140 keV) and the sum of 140 keV with the γ-ray energy of ^{99m}Tc (total ~160 keV) [11], which cannot be separated by the detector.

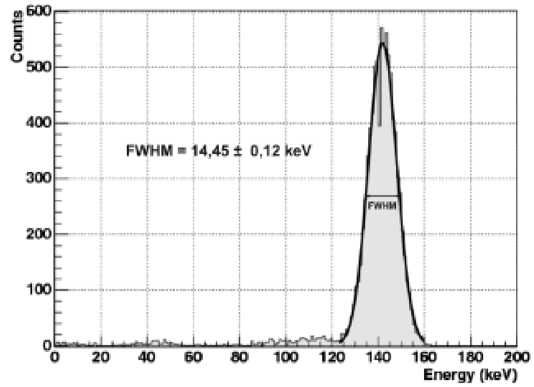

Figure 1 Simulated energy spectrum of a monoenergetic gamma point source of 140 keV with normal incidence on crystal without collimator.

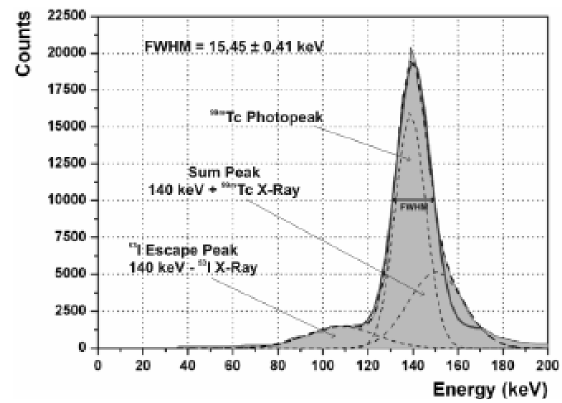

Figure 2. Experimental energy spectrum of ^{99m}Tc, decomposed on three Gaussian functions corresponding to different sum and escape energy peaks.

The results of fitting the peaks in both spectra by Gaussian functions gave a FWHM of 14.45±0.12 keV for the simulation and 15.45±0.41 keV for experimental data, corresponding to an energy resolution of 10.3±0.1 % for the simulation and 11.0±0.3 % for the experimental measurements. The manufacturer provides an upper limit of 9.9 % FWHM for the energy resolution at 140 keV.

2 - Sensitivity

The sensitivity of the gamma camera is determined by taking the ratio of the detected photons in the selection window to the total number of photons emitted in the solid angle of the FOV. The sensitivity, was experimentally measured and calculated by simulation for a ^{99m}Tc point source centered on FOV and located at the following distances from the detector with the LEHR collimator attached:0, 10, 15 and 20 cm. The experimental measurement was performed with a source activity of 1.9×10^6 Bq during 2 minutes whereas for the simulation 33 million photons were generated for each source position. The radioactive decay time was taken into account in experimental measurements and background radiation was subtracted. The results obtained for sensitivity for both simulations and real data are plotted in figure 3. & 4 for four source-collimator distances. The systematic higher sensitivity value obtained by the simulation is due to the acquisition dead time and signal overlap in the detector, which was not accounted for in the Monte Carlo.

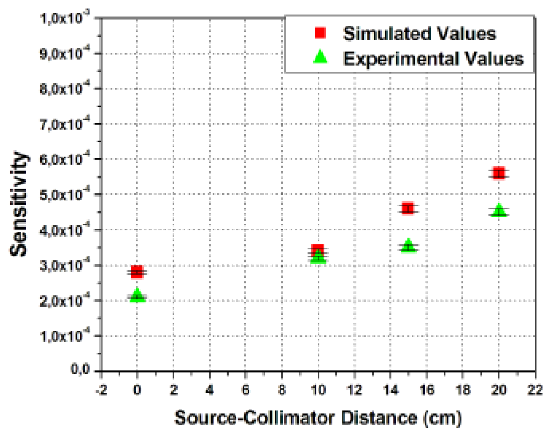

Figure 3 Comparison between simulated and experimental sensitivities for a ^{99m}Tc point source at four source-collimator distances.

3-Spatial Resolution

The experimental measurements were done using a 1.9×10^6 Bq 99mTc source with a diameter of 2 mm, placed at the center of FOV. Acquisitions for distances of 0, 10, 15 and 20 cm from source to the face of the LEHR collimator, 2 minutes each were obtained. The spatial resolution of the gamma camera was also obtained by Monte Carlo simulation using point spread functions (PSF) at the same distances as the experimental data.

The FWHM values of point spread functions of simulation and experimental measurements are presented in figure 4.. These values were obtained for four distances between the source and the collimator surface. We observed a difference between simulated and experimental results that is constant over the range of the source-collimator distance selected. This difference is due to the fact that the point source used in simulation is negligible extent compared to the 2 mm diameter source used in experimental measurements. For a source collimator distance of 10 cm, the simulated and experimental spatial resolution are 7.0±0.1 mm and 8.4±0.1 mm, respectively. The value provided by manufacturer for a point source at this distance is 8.3 mm [11], which nicely agrees with our experimental value.

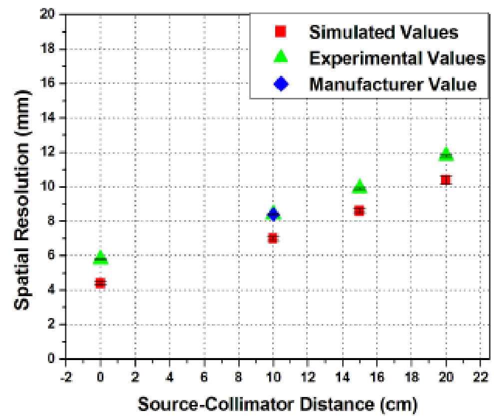

Figure 4. Comparison between simulated and experimental spatial resolution for a ^{99m}Tc point source located at four different distances from the collimator. The manufacturer value at 10 cm is also presented.

4- Phantom measurements

The phantom that were used in the first measurements was a large cylinder perspex phantom with a diameter of 21.5 cm and a height of 18 cm (Figure 5).

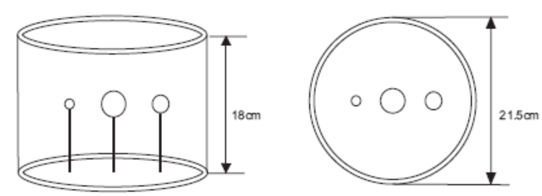

Figure 5: Dimensions of the cylindrical perspex phantom used in the first measurements.

Three spheres of different sizes were placed inside the phantom and attached by rods to the bottom of the cylinder. The volume of the spheres was 19.2 ml, 11.4 ml, and 5.7 ml respectively. The exact volume of the spheres was determined by weighing the spheres before and after filling them with thoroughly determined activity.

In the second part of the phantom measurements, a human-like phantom simulating the torso of a 70 kg man; a MIRD phantom, was used. The length of the torso phantom was 68 cm, width 40 cm, maximum thickness 20 cm and the volume was 40 liters. Into this torso phantom, lung-, heart-, kidney- and liver phantoms were placed. A plastic tube filled with water, (and later with activity), was placed over part of the liver to simulate an overlapping structure. The size of the organ phantoms was determined so that the replacement volume of them could be established. This volume could then be subtracted from the total volume of the torso phantom in order to determine the amount of water surrounding the organs.

Activity was added to this surrounding water in various concentrations to make a simulation of background activity. The lung phantoms were filled with Styrofoam beads in order to simulate the lower density of lung tissue and yielding an attenuation corresponding to the attenuation in normal lung tissue. The length of the lung phantom was 25 cm, the maximum width 15.5 cm and the volume was 2.26 l. The lung phantom also included a plug which volume was 140 ml. So the total replacement volume of one lung was 2.4 litres.

Two small cylinders simulating the kidneys were used. Each of the cylinders had a diameter of 6 cm and a length of 7.7 cm.

IV RESULTS AND DISCUSSIONS

1.1 Narrow beam attenuation coefficient

To obtain the narrow beam attenuation coefficient for the correction factors used in the Kojima background correction method, a number of values for μ_0, (for H_2O), were taken from the NIST website [11]. These values were tabulated in table-1 with μ_0 as a function of photon energy.

Table 1: Narrow beam attenuation coefficients for photon energies between 60 and 300 keV.

Energy (KeV)	μ_0
60	0.2059
80	0.1837
100	0.1707
140	0.1536
150	1.1505
159	0.1471
200	1.1370
300	0.1186

1.2 Effective attenuation coefficient

The effective attenuation coefficient for ^{57}Co was calculated for each organ and transformed to the effective attenuation coefficient for ^{99m}Tc.

The attenuation coefficients for each organ are presented in Table 2 below.

Table 2: Effective attenuation coefficients for the different organs in the MIRD phantom.

Phantom	μ_{effco}	μ_{effTc}	μ_{effI}
Liver	0.132	0.126	0.121
Kidneys	0.127	0.121	0.116
Heart	0.137	0.131	0.125
Intestine	0.129	0.124	0.118

1.3 Cylinder phantom measurements

The three spheres were filled with an amount of activity of 5.1 MBq, 3.1 MBq and 1.5 MBq of ^{99m}Tc respectively, (figure 5 shows the activity distribution in the phantom). In the cylinder phantom measurements four different combination of corrections were made: a) solely attenuation correction, b) attenuation- and Gates background correction, c) attenuationand Kojima background correction, d) attenuation- and Bujis background correction, showing an underestimation in the activity quantification of 9 - 30 % (Table 3).

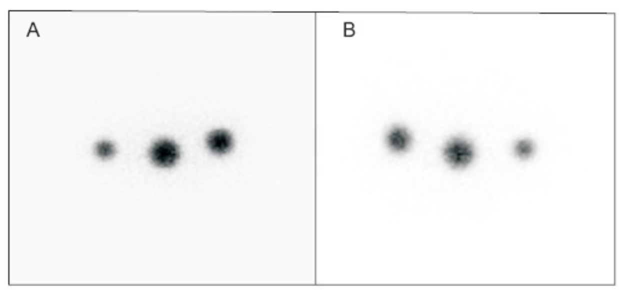

Figure 5: A: Anterior and B: posterior image from emission measurements of the cylindrical phantom containing three ^{99m}Tc-filled spheres of various size.

Table.3 : Deviation of calculated activity from true activity in emission measurements on cylinder phantom.

Method	Sphere 1 (19 ml)	Sphere 2 (11 ml)	Sphere 3 (6 ml)
Attenuation	-29%	-10%	-10%
Att, + Gates	-30%	-12%	-13%
Att. + Kojima	-27%	-9%	-10%
Att. + Bujis	-27%	-9%	-10%

V DISCUSSION

To perform an accurate quantification of the organ activity content from planar gamma camera images, several corrections has to be made. Two important factors that influences the results of the quantification is the attenuation and the scattering of photons in the organs and surrounding tissue. In this study, one method of attenuation correction and three different methods of scatter correction were used, (TEW, DEW and LEW). These methods have been studied among others by Ljungberg et al. [9], which showed that the use of the DEW method generated a complication, which was the choice of k-value used. The generally accepted k-value of 0.5 was used in the study of Ljungberg, as in this present study. The TEW method, which included two scatter windows of equal width intended to be more sensitive to noise, and thus a less accurate method than the LEW method in which the upper scatter window was set to zero and the lower window was used as in the TEW method. The results of that study showed that the TEW method greatly overestimated the scatter in the phantom and the LEW method underestimated the scatter but was more accurate.

In this study, the TEW method overestimated the scatter and thus underestimated the activity in the liver phantom. The LEW method gave an overestimation of activity to a lesser extent than for the TEW method. When considering large organs as the liver, and using ^{99m}Tc, the DEW method seemed to be the most accurate method for scatter correction, (-3%). Since this larger organ produces more scatter, one could expect the DEW method to be the most accurate as it subtracts the largest amount of scatter from the main window. But for the smaller organs, the kidneys and especially the heart, the use of the LEW scatter correction method showed great accuracy, (1.5% for ^{99m}Tc and zero background). The LEW method has, as mentioned before, shown more accurate results than the TEW method for measurements with ^{99m}Tc.

In a study by Delpon et al. [7] a comparison between the TEW and the DEW method showed that for small patients, the DEW method was more accurate than the TEW method and for average sized patients, the TEW was slightly more accurate than the DEW method.

The ^{123}I-measurements did not give the same results as the ones achieved for the ^{99m}Tc-measurements. The reason could be the difference in characteristics between the two radionuclides. In the ^{123}I decay, several high energy photons are emitted, which causes a larger amount of scatter in the higher energy window. This could explain that the deviation from the true activity values for the liver were highest when using the LEW method, (50%),

because when setting the higher energy window to zero, a large amount of scattered photons might not be taken into account. The deviation from the true activity values was lower for the TEW method, (43%), and the most accurate method in this case were the DEW method, (31%).

The activity was overestimated to a lesser extent in the heart with the LEW method as the most accurate method with an overestimation of 19%.

The most accurate activity value was obtained for the kidneys and the LEW method, which gave an overestimation of 6%. With respect to quantification with the three scatter correction methods, the LEW is the most accurate method when quantifying activity in small organs. The least accurate method for smaller organs was the DEW method. A reason that the LEW method showed more accurate results in this case than the DEW method (with ^{123}I), could be that both the correction methods lack the higher energy window, and the DEW method subtracts a larger amount of scatter than the LEW method. In organs as small as the kidneys, the amount of scatter is overestimated by the DEW method.

Correction for background activity was done by three different correction methods: the conventional background correction method, (Gates), the Kojima correction method and the Bujis correction method. The Gates, Kojima and Bujis correction methods were studied and compared by Bujis et al. [5], but with no scatter correction as in this study. The results of the Bujis study showed that the Kojima method was the most accurate method for quantification of activity in the kidneys, the Bujis method showed only slightly less accurate results and the conventional background subtraction greatly underestimated the activity in the kidneys.

For zero background activity, in this study the Bujis method was the most accurate for all of the organs when using ^{99m}Tc. When studying the Bujis and each of the three scatter correction methods, it was found that the combination of Bujis and LEW gave the most accurate results: -1.3% for the liver, 1.6% for the kidneys and -0.6% for the heart.

When the background activity was increased to a ratio of 10:1, the Kojima and LEW methods made the best set of correction methods regarding the kidneys with an overestimation of activity of only 2.6% for ^{99m}Tc. Regarding the heart, the three background correction methods gave similar results when used with the DEW method, but the Gates method were more accurate, (-5%). The TEW method were the most accurate for the liver and combined with the Bujis method it resulted in an underestimation of only 1%.

For higher background activity, (^{99m}Tc), the Bujis method showed more accurate results for the heart (-5.3%) especially together with the LEW scatter correction method, but for the liver, the LEW method combined with the Kojima method gave the most accurate results (-18%). For the kidneys the Gates method combined with the DEW for scatter correction gave an activity value that deviated from the true activity value with -10%.

At background concentration ratio of 10:1, (^{123}I), the Kojima method is more accurate than the other background correction methods. In combination with the LEW method, a difference of -2.6% was found.

References:

[1] Anger HO: Scintillation camera. Rev Sci Instr 29: 27-33, 1958.

[2] Cassen B, Curtis L, Reedc, Libby R: Instrumentation for ^{131}I use in medical studies. Nucleonics 9:46-50, 1951.

[3] Wrenn FR, Good ML, Handler P: The use of positron-emitting radioisotopes for the localization of brain tumors. Science 113: 525-527, 1951.

[4] Harper PV, Beck R, Charleston D, Lathrop KA: Optimization of a scanning method using technetium-99m. Nucleonics 22:50-54, 1964.

[5] Phelps ME, Hoffman EJ, Bujjs NA, Ter Pogossian MM: Application of annihilation coincidence detection of transaxial reconstruction tomography. J Nucl Med 16: 210-215, 1975.

[6] Kuhl DE, Edwards RQ, Ricci AR, et al: The Mark IV system for radionuclide computed tomography of the brain. Radiology 121: 405-413, 1976.

[7] Dolpan Rogers WL, Clinthorne NH, Shao L, et al: SPRINT II: A second-generation single-photon ring tomography. IEEE Trans Med Lmag 7:291-297, 1988.

[8] Genna SG, Smith AP: The development of ASPECT, an annular single-crystal brain camera for high-efficiency SPECT. IEEE Trans Nucl Sci 35:474-480, 1988.

[9] Ljungberg Rowe RK, Aarsvlod JN, Barrett HH, et al: A stationary hemispherical SPECT imager for three-dimensional brain imaging. J Nucl Med 34:474-480, 1993.

[10] Data sheet of Skylight Philips Dual Head gamma camera ,

[11] Website. National institute of standards and technology, NIST.

[12] Lena Jönsson, Michael Ljungberg, Sven-Erik Strandh. Evaluation of accuracy in activity calculations for the conjugate view method from Monte Carlo simulated scintillation camera images using experimental data in an anthropomorphic phantom. J Nucl Med 2005; 46:1679-1686.